catalysts

MDPI

Article

Surface Probing by Spectroscopy on Titania-Supported Gold Nanoparticles for a Photoreductive Application

Matteo Compagnoni [1], Alberto Villa [1], Elnaz Bahdori [1], David J. Morgan [2], Laura Prati [1], Nikolaos Dimitratos [2], Ilenia Rossetti [1] and Gianguido Ramis [3,*]

1 Dipartimento di Chimica, Università degli Studi di Milano, INSTM Unit Milano-Università and CNR-ISTM, via C. Golgi, 19, I-20133 Milan, Italy; matteo.compagnoni.chemistry@gmail.com (M.C.); alberto.villa@unimi.it (A.V.); 713578@unige.it (E.B.); Laura.Prati@unimi.it (L.P.); ilenia.rossetti@unimi.it (I.R.)

2 Cardiff Catalysis Institute, School of Chemistry, Cardiff University, Main Building, Park Place, Cardiff, CF103AT, UK; MorganDJ3@cardiff.ac.uk (D.J.M.); DimitratosN@cardiff.ac.uk (N.D.)

3 Dipartimento di Ingegneria Civile, Chimica e Ambientale, Università degli Studi di Genova and INSTM Unit Genova, via all'Opera Pia 15A, I-16145 Genoa, Italy

* Correspondence: gianguidoramis@unige.it; Tel.: +39-010-353-6027

Received: 12 November 2018; Accepted: 29 November 2018; Published: 5 December 2018

Abstract: The continuous increase in scientific reports concerning photocatalysis and in particular CO_2 photoreduction in recent years reveals the high degree of interest around the topic. However, the adsorption and activation mechanisms of CO_2 on TiO_2, the most used photocatalyst, are poorly understood and investigated. Gold nanoparticles were prepared by a modified deposition-precipitation method using urea and a chemical reductant. Bare P25 was used as reference. Combined spectroscopic investigations of fresh and spent samples with photoactivity studies reported in this article provide new insights to the role of CO_2 adsorption and carbonate formation on Au/TiO_2 during CO_2 photocatalytic reduction. The key intermediates' and products' adsorption (CO, methanol, ethanol) was studied, coupled with X-ray photoelectron microscopy (XPS) and UV-Visible spectroscopy. The adsorption of CO_2 on fresh and spent catalysts changes radically considering the carbonate formation and the gold surface presence. Methanol and ethanol revealed new adsorbed species on Au with respect to bare titania. The characterisation of the spent catalysts revealed the good stability of these samples.

Keywords: CO_2 reduction; diffuse reflectance infrared Fourier transform spectroscopy (DRIFTS); photoreduction; protoreactor; gold; Titania; photocatalysis; high pressure

1. Introduction

In order to contain the emissions of greenhouse gases, CO_2 photoconversion is one of the most intriguing processes from both an applicative and scientific point of view. In recent years, numerous reports relating to photocatalytic reduction of CO_2 under UV and visible light irradiation have been presented [1–3]. However, the photoreduction mechanism is still a matter of debate, even for TiO_2, which is the most studied photocatalyst. In particular, the CO_2 adsorption and activation mechanism (an important preceding step in CO_2 reduction) is not clear. For instance, Liu et al. investigated engineered oxygen-deficient blue TiO_2 nanocrystals for CO_2 photoreduction under visible light using diffuse reflectance infrared Fourier transform spectroscopy (DRIFTS) analysis, revealing different activity depending on the exposed facets, but without completely clarifying the adsorption and reaction mechanisms for the whole material [2]. By contrast Li et al. revealed how the presence of different

crystalline phases influence the photoreduction process, detecting the presence of unique interfacial trapping sites and possibly photocatalytic "hot spots" [4].

A comprehensive study of high pressure CO_2 photoconversion was carried out in one of our previous papers in order to shed light on the complex reaction mechanisms that occur both in the liquid and gas phases [5]. In such cases, a TiO_2-P25 photocatalyst was chosen as a reference material and products' distribution was compared after different reaction times and pH conditions. Two parallel reaction pathways were observed: (i) the first one involving the photoreduction of molecular carbon dioxide to formic acid, formaldehyde, and methanol, which may further evolve to gas phase products (photoreforming); (ii) the second one implying the reduction of carbonates to give formaldehyde and possibly methanol, or formic acid/reformate as a further consecutive step.

However, the choice of TiO_2 as a photocatalyst for CO_2 reduction is difficult, due to the lack of photoresponse under visible light irradiation and high electron-hole recombination rate. Its light absorption onset starts at wavelengths shorter than 380 nm as a consequence of the wide band gap [6], just in the border between the UV and the visible region. Solar light contains only 4% of the energy in the UV region able to promote photoexcitation of titania, therefore a large proportion of the light is useless, limiting the efficiency of the process. The extension of the photoresponse towards the visible region can be achieved by metal doping [6], doping by non-metallic elements with creation of oxygen vacancies [7] and, more recently, by deposition of noble metal nanoparticles (NPs) with a surface plasmon band, particularly Au [8], Ag [9], or doping with metal-organic molecules [10].

The addition of a metal or dopant further increases the complexity of adsorption and activation mechanisms during the process. Tahir et al. investigated how the surface plasmon resonance excitation influences the reaction pathways using Au/Ag nanoparticles on TiO_2 nanowires [3]. The excited electrons in the Au/Ag are injected into the conductance band of TiO_2, making them react easily with CO_2 and H^+ radicals, forming CO, CH_3OH, and CH_4.

Moreover, the deposition method of the metal or dopant deeply affects the resulting material and its performance, e.g., gold nanoparticles supported on oxides [11,12]. Morphology, size, metal oxidation state, and metal-support interaction deep modify activity and/or the selectivity of the whole catalyst. Therefore, a lot of attention has been paid to the preparation of gold catalysts in order to assess as much as possible the relation between preparation method and characteristics of the produced materials. Dimitratos et al. reported a detailed study concerning the effect of preparation method (deposition-precipitation versus sol immobilisation method) and reduction method (calcination versus chemical reduction) on Au/TiO_2 catalysts for the liquid phase oxidation of glycerol [12]. The work demonstrated the crucial role of Au oxidation state and gold particles' dimensions depending on the method and conditions adopted. In another work, Villa et al. reported an alternative sol immobilization route for the deposition of Au on TiO_2 [13]. Recently, we investigated an innovative modified deposition/precipitation method for the preparation of supported gold nanoparticles [14]. This promising synthetic route involves the use of urea as a basic agent and $NaBH_4$ as a chemical reductant, in contrast to the traditional high-temperature reduction step. A deep spectroscopic investigation combined with other traditional characterisation techniques has deepened our understanding of this modified gold deposition strategy.

In previous works, we applied this technique for the synthesis of Au/TiO_2 samples and tested them for CO_2 photoconversion by tuning pressure, temperature, and pH [15,16]. The operating conditions were then selected to maximise the production of gas phase products, i.e., CH_4 + H_2, with respect to liquid phase organic compounds. However, also in these cases, the adsorption and activation mechanisms remain unclear.

The adsorption process is fundamental for photocatalytic applications, CO_2 photo-conversion included. Delavari et al. explored the gas phase reaction using immobilized TiO_2 nanoparticles' semiconductor on stainless steel mesh [17]. The Langmuir-Hinshelwood model was applied to the reaction network and revealed that yield rates of products were highly dependent on efficient adsorption of the reactants and desorption of products over the catalyst surface.

As mentioned, a robust and already deeply investigated modified deposition-precipitation method was adopted in this work for photocatalyst preparation, in order to study the CO_2 adsorption pathways and the interaction mechanisms with the common reaction products for different Au loading. The characterization of TiO_2 surface and Au nanoparticles was carried out to interpret reactivity and deactivation of photocatalysts for the reduction of CO_2 in aqueous medium.

2. Results and Discussion

Activity testing of the catalysts revealed a significant productivity for methanol (up to ca. 1.5 mol/h·kg_{cat}, which is a very significant result when compared to the literature) and some methane formed in the gas phase (ca. 0.3 mmol/h·kg_{cat}) only when using gold-loaded TiO_2-P25 samples. The productivity of all species increased while increasing the gold content from 0.1 to 0.2 wt. %, then remaining quite constant for a further increase of the metal. H_2 + CO also formed, thanks to a consecutive reaction step of photoreforming, with the highest H_2 amount attesting to ca. 18 mmol/h·kg_{cat}. The comparison with the bare, unpromoted semiconductor revealed that the main products were HCHO and HCOOH, with only traces of methanol and no CH_4 [18]. Therefore, we undertook an investigation on the role of gold for the activation of CO_2 during photoreduction and methanol for the consecutive photoreforming step. The results are reported in the following sections.

2.1. Morphologic and Electronic Characterization

Morphologic and electronic characterizations have been widely reported elsewhere [14]. Briefly, high-resolution transmission electron microscopy (HRTEM) and scanning transmission electron microscopy (STEM) have confirmed that adopting the deposition-precipitation method led to very narrow gold particle size distribution fitted by a log-normal curve, with a mean diameter between 3.7 and 4.6 nm. In addition, the nature of the gold species was clarified by X-ray photoelectron microscopy (XPS). The Au4f XPS spectra of Au/TiO_2 samples presented the characteristic 4f7/2 and Au 4f5/2 transitions doublet of the two spin–orbit components. Evaluation of the oxidation state of Au, using the binding energy (BE) of the Au 4f7/2 peak, confirmed the well-dispersed and metallic form of gold (Au^0) (BE = ca. 83 eV) without any detectable Au^{n+} species (BE = ca. 85.5 eV).

2.2. DR UV-Vis Spectra

For metal nanoparticles of Au^0, Ag^0, and Cu^0, the plasmon absorption arises from the collective oscillations of the free conduction band electrons that are induced by incident electromagnetic radiation. The study of gold plasmonic bands is an interesting point because their absorption frequency is very sensitive to changes in the environment and material structure [19,20]. This investigation was carried out by UV-vis diffuse reflectance absorbance spectroscopy, looking for increased UV absorption with increasing Au content. UV-vis spectra are exhibited in Figure 1. Visible light absorption of TiO_2 photocatalysts remarkably enhance with the increase of the gold percentage, due to the surface plasmon resonance (SPR) effect of Au-NPs, indicating that the metallic Au exists in the sample, as already confirmed in XPS analysis and DRIFTS analysis [14]. The visible light absorption of Au-NPs culminates in a broad response, ranging from 450 to 700 nm, which is possibly due to size distribution of Au-NPs. The wavelength at the maximum of the SPR band (λmax) is located at 553 cm^{-1}. For Au/TiO_2 samples, the intensity of absorbance band is related to the size and content of the Au particles. The progressive increase of intensity with metal loading and the equal particle size dimension detected by CO-DRIFTS and microscopies [14] suggests a very specific metal deposition with no alteration of metal size, charge, and morphology.

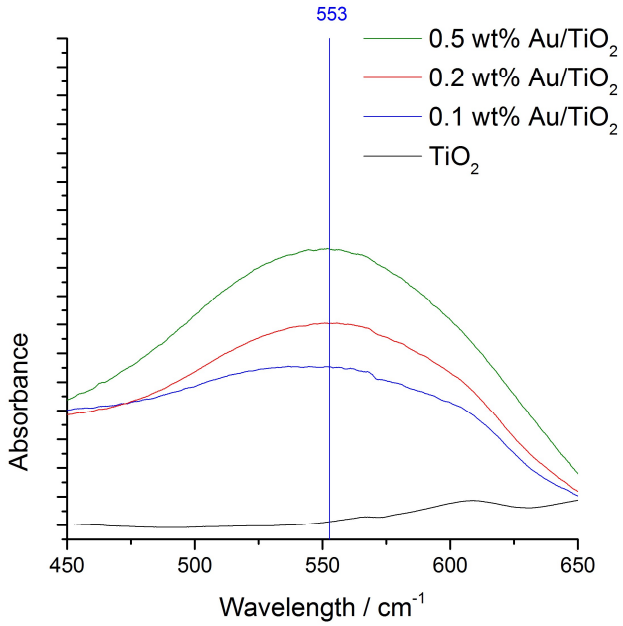

Figure 1. Enlarged UV-vis region of spectra for surface plasmon resonance band of Au/TiO_2 photocatalysts changing the gold loading.

2.3. CO_2-DRIFTS

The adsorption of CO_2 on TiO_2 represents the preceding step of the photoreduction reaction, however, its study has been scarcely reported. Few articles have been published considering the nature of CO_2 adsorption coupled with advantages and drawbacks from a photocatalytic point of view. This is also true for some of the most studied photocatalysts, such as TiO_2 [21–23]. Computational calculations indicated that electron transfer to CO_2 can be mediated by surface defects and factors such as phase components (e.g., rutile, anatase) [24].

In this work, DRIFT spectroscopy was applied in the first stage to identify the CO_2 adsorption species and reaction intermediates, investigating how the addition of gold nanoparticle influences the process. CO_2-DRIFTS spectra are reported in Figure 2. Spectroscopic studies help to unravel mechanism details and changing behavior of the surface catalyst atoms [25,26]. Observing the spectra of the 4 different samples, by comparing the relative intensities of the bands (rather than their absolute value, which is not comparable according to the Lambert Beer law for samples different in surface area, density, amount loaded, etc.), it is possible to obtain significant quantitative data on the amount of the adsorbed species.

CO_2 adsorption gives rise to several IR bands in the range of 1800–1000 cm^{-1}. Three main peaks at 1312, 1416, and 1577 cm^{-1} were detected, with a shoulder at higher frequency near 1675 cm^{-1} for the latter. Moreover, further weaker components are detectable. According to the bibliography, a possible attribution was carried out as reported in Table 1.

One of the main species involved in the CO_2 photoreduction process is the carbon dioxide anion radical formed during the reaction mechanism:

$$CO_2 + e^- \rightarrow CO_2^- \rightarrow E_{redox} = -1.9 \text{ eV (vs. NHE) [8]}$$

The transfer of an electron from the surface to the adsorbate can also occur without irradiation, simply during the adsorption [27]. Surface Ti^{3+} centers activate CO_2 in this way, forming bands characterized by small $\Delta\nu$ and placed around 1670 and 1310 cm^{-1} [27].

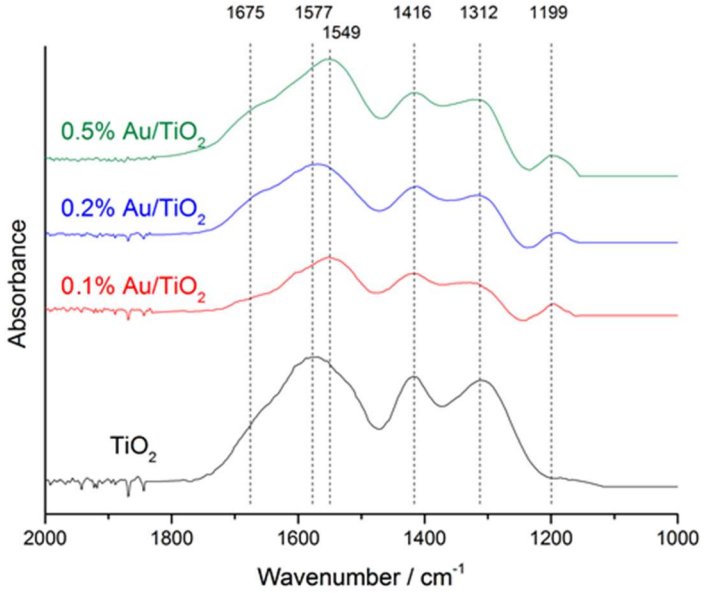

Figure 2. Diffuse reflectance infrared Fourier transform spectroscopy (DRIFTS) spectra of CO_2 interaction with gold supported photocatalysts.

Table 1. IR main bands assignment for Au/TiO_2 Samples.

Species	ν (cm^{-1})	Ref.
CO_2 bent species	1312, 1675	[25]
Bicarbonate species HCO_3^-	1416, 1500–1600	[26,27]
Bidentate carbonate (b-CO_3^{2-})	1577–1549	[28–31]

The formation and attribution of bidentate carbonate is in accordance with László et al. and their studies on photocatalytic CO_2 and CH_4 conversion over Au- and Rh-doped titanate nanotubes [28]. However, any peak of monodentate formate ($HCOO^\bullet$) cannot be ruled out in our spectra (bands at 1585 and 1384 cm^{-1}). This can be explained considering the reaction mechanism of CO_2 photoconversion, because this species is generated only after the reaction between the $CO^{\bullet-}{}_2$ radical anion and hydrogen ion (Equation (1)), and in dark conditions the anion is not present.

$$CO^{\bullet-}{}_2 + H^+ \rightarrow HCOO^\bullet \quad (1)$$

Liu and co-workers reported the strong correlation between the reaction mechanism and the carbonate species generated during the initial adsorption in dark conditions [29]. This occurs because of the different behaviors of $CO^{\bullet-}{}_2$ depending on the carbonate species formed over the surface. In their case, the brookite polymorph revealed a carbonate more reactive than anatase, and the comparison between the dark DRIFTS analysis revealed a stronger presence of HCO_3^- and m-CO_3^- in the case of brookite. However, a new discussion point arose, because in our study analysis was performed on P25, which is a mixture of anatase and rutile (78% and 22% respectively). The nature of the present carbonate form is related to the crystalline form, however IR spectra of adsorbed probe molecules supply information mainly from the surface, while XRD gives information mainly from the bulk. Su et al. revealed the b-CO_3^{2-} symmetric mode peak for anatase but not for rutile with a higher peak for surface bicarbonate (HCO_3^-) regarding the rutile form [30]. Additionally, the band at 1589 cm^{-1} is the strongest one when CO_2 is adsorbed on anatase, while in the case of rutile, the band at 1416 cm^{-1} is the strongest one. This is in accordance with our analysis, which represents exactly our mixed situation with commercial P25.

Another key point is the adsorption competiveness between CO_2 and H_2O. The role of water is important either in gas and liquid conditions. For instance, Chen et al. detected a stronger increase of methane yield (~12% CO_2 conversion) by increasing the CO_2 to water ratio using mixed-phase titania nanomaterials [31]. Water is the reductant reagent of the photoreaction. A proper experiment under dry and wet conditions was performed (Figure 3), with the same peak location and band shape of the spectra in Figure 2. A marked increase of the relative intensity of band 1312 and 1675 cm^{-1} was detected (i.e., peak height subtracted by the baseline of the spectra). This result is crucial: it shows that H_2O promotes the formation of the CO_2 radical anion, with a synergistic effect for CO_2 photoreduction.

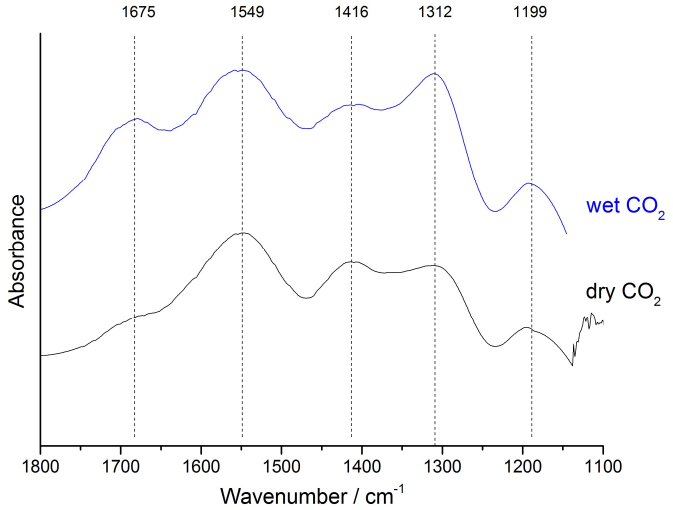

Figure 3. DRIFTS spectra of CO_2 and H_2O interaction on 0.5 wt. % Au/TiO_2: CO_2 adsorption saturated with water (wet CO_2) and not (dry CO_2).

This analysis also allowed the study of the influence of hydroxyls groups. The identical relative intensities of typical bands associated with hydroxyls in wet and dry conditions confirm that the hydroxylation does not change at all compared to the effect of Figure 3.

The band at 1199 cm^{-1} was present just for the gold samples, as reported in Figure 2. This aspect is very interesting, because it showssome carbonate formation associated only with gold. The band was associated with a particular bicarbonate formation detected also for other Au-based catalysts in accordance with Neatu et al. [32,33]. The corresponding band is located between 1500–1600 cm^{-1}, so not clearly detectable, because of the overlapping. This can be confirmed by observing the comparison of peak relative intensities (i.e., peak height subtracted by the baseline of the spectra). In particular, the intensity of the peak at 1549–1579 cm^{-1} is the highest in the case of bare TiO_2, with a relative decrease of 20–60% for the gold samples. The absolute value of this decrease is comparable with the peak intensities of the bands at 1199 cm^{-1} for the gold samples.

The addition of gold provides evidence of a lower formation of bidentate carbonates, favouring higher concentration of surface bicarbonate species. The intensity of the latter band increases in wet conditions with respect to dry CO_2. This can suggest a possible promoting effect of gold, which plays a role in the activation of surface OH in CO_2 adsorption.

The intensity of the band at 1199 cm^{-1} increases in wet conditions with respect to dry CO_2.

2.4. DRIFTS of Adsorbed Methanol and Ethanol

Another key point is the evaluation of products and reagents during the photoreactions. Methanol is one of the main products of the process [34,35] and is also the key compound for the subsequent photoreforming step [5]. With the aim of identifying surface species that were formed during methanol adsorption and that can be considered for the mechanism assumptions proposed in literature, several

DRIFTS analyses using methanol as probe molecule were carried out. The spectra are shown in Figure 4A,B.

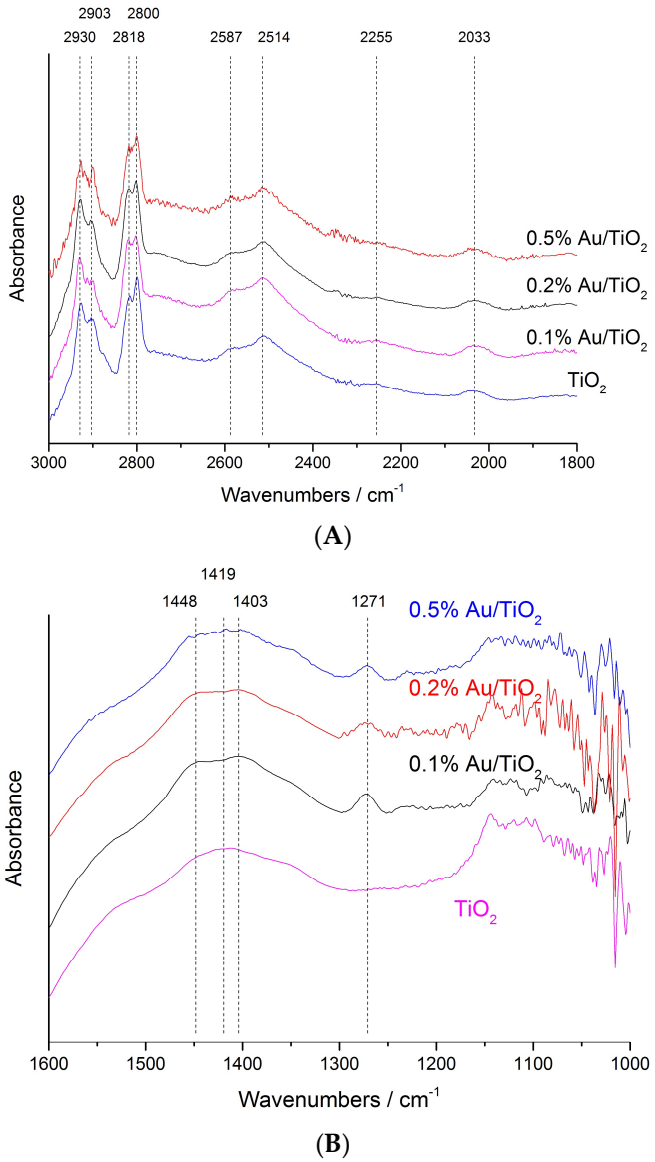

Figure 4. (**A**) DRIFTS spectra recorded as a TiO_2-supported gold sample was treated in flowing mixtures of methanol and N_2 in 3000-1800 cm^{-1} spectral region. (**B**) DRIFTS spectra recorded as a TiO_2-supported gold sample was treated in flowing mixtures of methanol and N_2 in 1600–1000 cm^{-1} spectral region (down).

In addition to the C–H stretching bands in the region between 2800–3000 cm^{-1}, characteristic alkoxy surface species $–OCH_3$ were detected in not well-resolved spectral region around 1100 cm^{-1} [36–38]. An important role of the methoxy species was attributed by Greaves et al. [39], assuming their direct involvement in the photoreforming mechanism, especially in the presence of gold. The kinetic mechanism proposed considers the methanol adsorption at free sites on gold nanoparticles and subsequent formation of a methoxy intermediate, which is stable in the absence of light and blocks the reaction. In the presence of light, the photo-generation of holes induces the formation of the high oxidative hydroxyl radical, which reacts with the methoxy species and forms CO_2 and H_2O. The adsorption mechanism on Au/TiO_2 proceeds accordingly with the following mechanisms [39]:

(a) $CH_3OH \rightarrow CH_3OH^*$

(b) $CH_3OH + O^{2-}{}^* \rightarrow CH_3O^-{}^* + OH^-{}^*$

(c) $CH_3OH^* + OH^-{}^* \rightarrow CH_3O^-{}^* + H_2O + V_o{}^{2-}$

Where * denotes the species adsorbed on the TiO_2 surface and $V_o{}^{2-}$ anion vacancies. In Figure 4 the presence of the bands at 2930 and 2818 cm^{-1} indicates that methoxy species are formed according to steps (b,c) above. The bands at 2930 and 2800 cm^{-1} correspond to the couple of $\nu_{sym}CH_3$ modes [38].

Therefore, our results confirmed that the band at 2930 cm^{-1} is relative to the methoxy species bonded to Ti^{4+} sites, while the presence of gold does not influence the nature of the adsorption process. However, the relative intensity of the peak at 2818 cm^{-1} is significantly lower in bare P25 compared to samples with gold, indicating a higher amount of $V_o{}^{2-}$ anion vacancies in presence of gold particles.

This aspect can be associated with the other big difference comparing the gold samples with the bare one (Table 2): the two additional peaks for the bands at 1448 cm^{-1} and 1271 cm^{-1}. A spectroscopic investigation by Martinez et al. performed using methanol and TiO_2-supported gold materials revealed the possible influence of metal loading and deposition method of gold [40]. They did not conclude that there is any influence of gold when comparing the spectra during the methanol adsorption. However, a very high metal loading was used (5 wt. %) and a deposition method involving $NaBH_4$ was carried out. By contrast, Calzada et al., studying gold samples prepared by deposition-precipitation method at low loading, like in our case, reported differences comparing the metal containing sample and the bare support [41], revealing the critical influence of gold present during methanol adsorption. So, according to K. Kähler at al., the band at 1271 cm^{-1}, associated with the band at 1448 cm^{-1}, was attributed to a carbonate formed on Au metal nanoparticles [42].

Table 2. IR main bands assignment for Au/TiO_2 Samples.

Surface Species	Frequency (cm^{-1})	Ref.
$\nu_{sym}CH_3$ modes of Methoxy on top on Ti^{n+}	2930–2800	This work, [36–38,43]
Carbonates due to Au	1448, 1271	This work, [42]

A less polar and hydrophilic alcohol, such as ethanol, was used for a comparison with methanol DRIFT spectra. The results are shown in Figure 5.

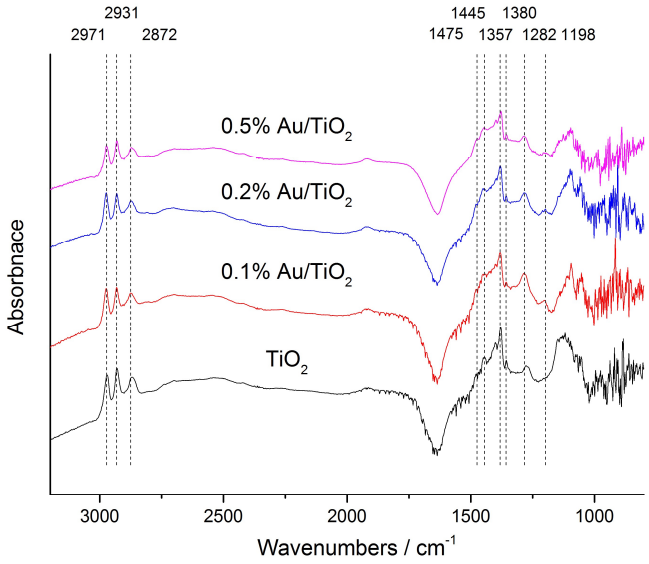

Figure 5. DRIFTS spectra recorded as a TiO_2–supported gold sample was sequentially treated in flowing mixtures of ethanol and N_2.

According to Gong et al. [44], the formation of the aldehyde is one of the first steps for ethanol decomposition. Alkoxy groups form in dark conditions upon ethanol adsorption. The identification of these alkoxy groups and their evolution on different oxidic surfaces, in our case TiO_2 and Au/TiO_2, is a key point.

$$CH_3CH_2OH \rightarrow CH_3CH_2O\text{-}Ti^* + OH^*$$

Formal charges are omitted for clarity. As in the case of methanol, a new band associated with carbonate on Au nanoparticles at 1198 cm^{-1} was present.

2.5. DRIFTS—OH Region

Surface OH groups can directly influence photoactivity performance. Indeed, OH groups are efficient carrier traps for the holes generated in the lattice by the absorption of light. The mechanism proposed is the following [45–47]:

$$Ti^{IV}\text{-}OH^- + h^+ \rightarrow Ti^{IV}\text{-}OH\cdot$$
$$Ti^{IV}\text{-}H_2O + h^+ \rightarrow Ti^{IV}\text{-}OH\cdot + H^+$$

In addition to the high oxidation potential, these radicals act as adsorption sites for many molecules, and therefore are fundamental for the initial CO_2 photoreduction process (high oxidation of the hole scavenger) and photoreforming of organic products.

DRIFT spectra under N_2 atmosphere were performed in order to study of surface hydroxyl groups of titania and the influence of metal loading. Two characteristic bands at 3693 and 3632 cm^{-1} were detected in the OH spectral region between 3400–4000 cm^{-1}. The higher frequency band is ascribed to terminal hydroxyl groups coordinated to Ti^{4+} sites, which are responsible for photocatalytic activity, while the lower is related to the bridged hydroxyl species [45,47].

No band at 3400 cm^{-1} was detected because of the absence of water in the nitrogen flow (this band is usually reported and attributed to hydrogen-bonded water in interaction with surface hydroxyl groups) [47,48]. A slight attenuation of the higher band intensity was observed for the sample with the highest Au loading. This effect was reported to be more marked by Orlov et al. and was attributed to the partial elimination of hydroxyl groups [48]. However, their study was performed comparing a very different metal loading (from 0.42 to 5.58%).

The experimental analysis confirmed the low influence for the surface hydroxylation of such a percentage in weight of gold on high surface area titania.

2.6. XPS-Fresh Catalyst (O Region, Ti Region)

In order to investigate how the surface hydroxyl species change after gold deposition treatment and the related photoactivity of the materials, X-ray photoelectron spectroscopy was adopted as complementary investigation technique. XPS gives information on valence of elements on and near the surface of photocatalysts. As shown in Table 3, OH/lattice oxygen ratios are quite similar, although a slight decrease of the value with increasing the gold loading reveals less OH groups.

Table 3. XPS Analysis of the surface composition of fresh samples.

Sample	Au 4f	O 1s (Lattice)	O 1s (OH)	Ti 2p	OH/Lattice O	Ti/O (Lattice) Ratio
0.1% Au/TiO_2	0.04	36.49	5.11	18.61	0.14	0.51
0.2% Au/TiO_2	0.05	35.22	4.69	17.71	0.13	0.50
0.5% Au/TiO_2	0.09	36.87	4.38	18.51	0.12	0.50

The nature of the negative charge on gold is closely related to support [49], in particular regarding the charge transfer between gold particles and M^{3+} cations of the support lattice. Many studies have pointed out that defect sites (e.g., oxygen vacancies) might play an important role in charge transfer for the formation of negatively charged gold.

The Au 4f XPS spectra of Au/TiO_2 samples are shown in Figure 6, where the characteristic doublet of the two spin–orbit components are visible ($4f_{7/2}$ and Au $4f_{5/2}$ transitions). The oxidation state of Au at the surface of the catalyst was evaluated by analysing the values of binding energy (BE), referring to the Au $4f_{7/2}$ peak.

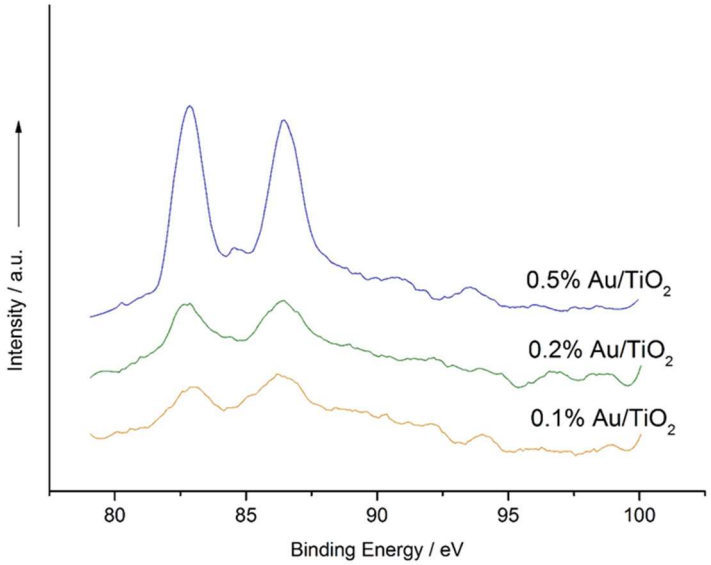

Figure 6. XPS spectra of Au 4f region for 0.1 wt. %, 0.2 wt. % and 0.5 wt. % Au/TiO_2 samples.

2.7. Spent Photocatalyst Characterization

Deactivation is a general problem in heterogeneous processes, due to the accumulation of intermediate products or products on the TiO_2 surface [50]. The deactivation can be reversible or irreversible. Blount et al. investigated the photocatalytic oxidation of toluene in gas phase using Pt/TiO_2-P25 and detected a deactivation, due to the less reactive intermediate produced during the reaction, such as benzoic acid [51]. Regarding CO_2 photoreduction, very few papers can be found talking about deactivation phenomena. Deactivation from carbonaceous species formed during the photocatalytic reduction of CO_2 with water in gas phase was studied by Uner and co-workers using Pt/TiO_2 photo-catalysts [52]. Unfortunately, the carbon deposition over the photocatalyst surface was only identified by evaluating the methane formation in dark conditions in presence of hydrogen. Another critical intermediate or product, depending on the goal of the process, is carbon monoxide, because its presence can lead to a marked deactivation of the catalyst if the material composition is not properly tuned [53].

The photoactivity tests for these photocatalysts and the relative discussions were reported elsewhere [15], because in this work the focus was on bringing a contribution about the mechanisms and relevance of reagent and product adsorption/interactions with gold-loaded titania. Briefly, tests were carried out at 6 bar, basic pH (12), 80 °C, and a time reaction of 70–90 h [15]. To better clarify the critical aspects involved in the photoreaction mechanism, post-catalytic measurements were performed in order to investigate the variation occurred in the catalyst during the photoreaction. For instance, the formation of the strong reductant radical anion $CO_2\cdot^-$ can change the gold oxidation state during the test, representing a critical aspect because of the changing of the band gap or photoactivity efficiency. Although this aspect was detected for sulfide-based semiconductors during CO_2 photoreduction [54], its presence using TiO_2 seems unlikely due to the high resistance of the titania below UV irradiation, especially in the wavelength range used in this work.

The photocorrosion of the materials was found particularly relevant for reactions carried out in water and when the metal is deposited on its surface. The critical point is the metal leaching phenomenon involving the gradual deactivation of the catalyst, which can occur due to its continuous

metal oxidation/reduction cycles [6]. In addition the accumulation of the photo-generated holes in the valence band can be a photocorrosion source if a proper amount of hole scavenger is not used [55].

XPS was used to investigate the oxidation state of gold and carbon on the surface of the spent catalysts (Table 4). This aspect of photocorrosion was studied on the samples used for the longer kinetic tests (92 h), in order to stress the critical conditions for the photocatalyst.

Table 4. XPS binding energy of Au $4f_{7/2}$ region data and C atomic percentage for gold based catalysts before and after the photoactivity tests.

Sample	Au $4f_{7/2}$ BE Fresh (eV)	Au $4f_{7/2}$ BE Spent (eV)	C 1s, %at Conc Fresh	C 1s, %at Conc Spent
0.1 wt. % Au/TiO_2	83.6	83.0	39.59	36.14
0.2 wt. % Au/TiO_2	83.6	83.0	42.09	36.38
0.5 wt. % Au/TiO_2	83.6	83.0	39.99	41.93

XPS Au band analysis on a spent sample revealed the presence of metallic gold, and the absence of any charge modification, as proposed by other works on other photocatalytic conditions and processes [56].

The quantity of the surface carbon detected by XPS was very similar, without denoting any significant carbon deposition during the photoactivity tests. Therefore, in light of these results, it would be expected to obtain the same IR spectra after CO adsorption on the fresh and spent samples. For this reason, the charge and the dispersion of the gold nanoparticles were probed using carbon monoxide, combined with DRIFT spectroscopy (Figure 7). In a detailed previous article, the surface of these fresh materials was studied in depth using CO-DRIFTS for the CO oxidation reaction [14]. For all the Au/TiO_2 fresh samples, the presence of CO gave rise to one or two IR bands in the CO carbonyl spectral region (1950–2150 cm^{-1}). The highest frequency IR band (2106 cm^{-1}) was attributed to linearly adsorbed CO on metallic gold, while the broad and asymmetric band at lower frequencies, with the maximum located at 2072 cm^{-1}, was deconvoluted on the basis of a Gaussian model and the several overlapping peaks were attributed to the linear, multisite, and bridged CO on $Au^{\delta-}$.

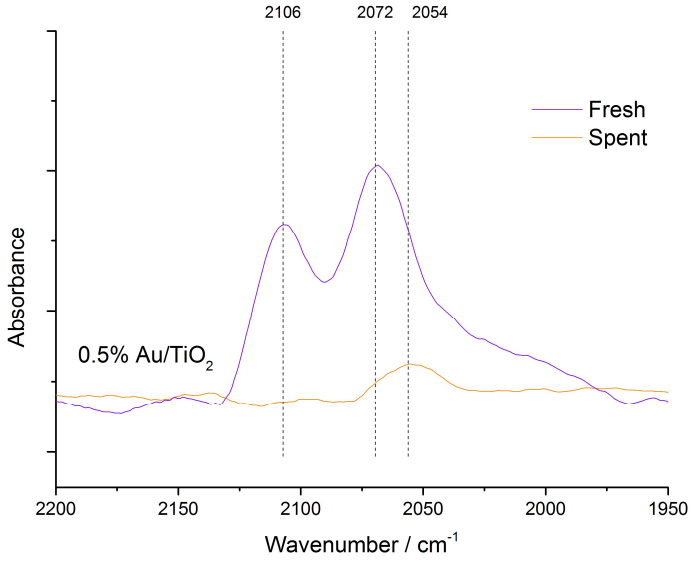

Figure 7. CO-DRIFT spectra over 0.5 wt. % Au/TiO_2 samples before and after the photocatalytic CO_2 reduction.

DRIFT analysis without probe molecules was then carried out on the spent samples in order to check the presence of CO, which is sometimes considered one of the deactivating compounds. The spectra, after the subtraction of the fresh analogues, revealed the formation of several species in the carbonate region, as shown in Figure 8. All spent spectra did not reveal CO chemisorbed or

physisorbed (peaks usually ascribed to the region 2017–1970 cm^{-1}) [37], leading to the conclusion that in liquid phase this deactivation mechanism is minor with respect the gas phase process. The CO generation occurs mainly due to the Ti centers of the oxidic support [57], because the other possible path (direct photolysis of CO_2) is very unlikely out of the deep UV irradiation conditions [6]. Another point supporting this result is the fact that CO is bound much more weakly to the Au surface due to the low energy of d orbitals in Au with respect other metals such as Pd [39].

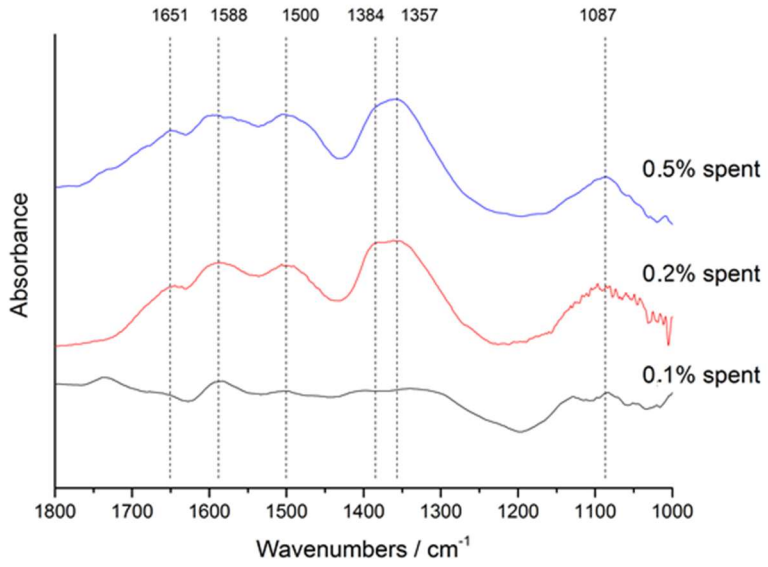

Figure 8. Carbonate IR region obtained after the subtraction of DRIFTS spectra of fresh samples to spent samples.

3. Materials and Methods

3.1. Preparation of Au/TiO2

The deposition-precipitation method was used to load Au nanoparticles (NPs) with urea and a chemical reductant (DP-UC). 1 g of TiO_2 (Evonik, Essen, Germany, TiO_2 P25, SA 50 m^2 g^{-1}) was suspended in distilled water (100 mL) and added to 5 g of urea (Aldrich, Saint Louis (MO, US, >99%). A solution of $NaAuCl_4 \cdot 2H_2O$ (Aldrich, 99.99%) was added and the mixture was stirred for 4 h at 353 K. The catalyst was filtered and repeatedly washed with water. The material was again suspended in distilled water and added at room temperature with a 0.1 M solution of $NaBH_4$ (Fluka, >96%) so to have $NaBH_4$/Au = 4 mol/mol [58]. The sample was filtered, washed, and dried at 373 K for 4 h. Au loading was analysed by Atomic Absorption Spectroscopy (AAS) analysis of the filtrate (Perkin Elmer, Monza (MB), Italy, mod. 3100), retrieving the nominal composition. Au/TiO_2 catalysts with the following composition were prepared: 0.1 wt. %, 0.2 wt. %, 0.5 wt. % Au/TiO_2. Bare P25 was used as a reference.

3.2. Characterization

Diffuse reflectance infrared Fourier transform spectroscopy (DRIFTS) was carried out by means of a Bruker (Coventry, CV4 9GH, UK) Tensor 27 spectrometer fitted with a HgCdTe (MCT) detector, a Harrick Praying Mantis HVC-DRP-4 cell equipped with two ZnSe windows, and operated with OPUS software. The DRIFTS cell was equipped with gas inlet and outlet and heating and cooling devices. 40 cm^3 min^{-1} of a 5% CO/N_2 gas mixture were fed through mass-flow controllers. Each spectrum is the average of 64 scans collected with a spectral resolution of 2 cm^{-1}. When CO_2 was used as a probe, a flow of 6 cm^3 min^{-1} of a 30% CO_2 in N_2 was fed in order to have the best comparable results. Each spectrum is the average of 64 scans collected with a spectral resolution of 2 cm^{-1}.

The ZnSe windows used cut off the spectrum below 650 cm^{-1}, therefore this region was not included in the discussion. The results are reported as absorbance, so in the reported spectra a positive increase of peak intensity indicates an increase of the amount of that species, whereas a negative one shows loss of moieties associated with that particular vibrational mode. All samples were ground before the analysis. The spectra are obtained after subtraction of reference background recorded under N_2 flow after heating the sample at 393 K for 30 min.

Diffuse Reflectance (DR) UV-Vis spectra were obtained by means of a Varian (Palo Alto (CA), US) Cary 4000 spectrophotometer including a Harrick Praying Mantis HVC-DRP-4 cell. The catalyst was placed in the cell and spectra were recorded under N_2 atmosphere, air, 1% CO/N_2 or 1% CO/air (50 mL min^{-1}).

X-ray photoelectron spectroscopy (XPS) was carried out with a Kratos (Manchester, M17 1GP, UK) Axis Ultra-DLD instrument with a monochromatic Al K_α X-ray source operating at a power of 144 W (12 mA × 12 kV) power. High resolution and survey scans were performed at pass energies of 40 and 160 eV, respectively. Spectra were calibrated to the C (1s) signal at 284.8 eV and quantified using CasaXPS and a modified Wagner sensitivity factors supplied by the manufacturer.

4. Conclusions

The characterization of TiO_2 surface and Au nanoparticles was carried out to interpret reactivity and deactivation of photocatalysts for the reduction of CO_2 in aqueous medium. Different modes of CO_2 surface adsorption have been observed upon Au loading. This can promote the activation of CO_2 during the photocatalytic process. Due to the formation of different reduction products towards methanol, the latter was also tested for surface adsorption. This information is important for interpreting the consecutive photoreforming step. The deposition of Au nanoparticles induced a significant plasmon resonance band, whose intensity increased proportionally with metal loading. CO_2 adsorbed in different coexisting forms on catalyst surface, i.e., CO_2, bicarbonate and carbonate species. The formation of the CO_2 radical anion was crucially improved by the presence of water. The presence of gold gave rise to a specific CO_2 adsorption feature, which likely is correlated to an activated state, based on the higher photocatalytic efficiency observed for these samples.

Methanol adsorption mainly occurs over TiO_2 sites, forming methoxy-species, which can be further oxidised in the consecutive photoreforming step. Carbonates over Au particles were contemporarily detected.

The characterisation of the spent catalysts revealed the good stability of these samples, which did not undergo any significant change of gold loading or oxidation state, nor important variation of the amount of C adsorbed on the surface (surface saturation).

Author Contributions: M.C., E.B. and D.J.M.: collection of experimental data for catalysts characterization; M.C.: writing—original draft preparation; A.V.: catalysts preparation; L.P., N.D.: supervision; I.R. and G.R.: writing—review and editing, funding acquisition, supervision, project administration.

Funding: The financial contribution of MIUR through the PRIN2015 grant (20153T4REF) is gratefully acknowledged (G. Ramis and I. Rossetti). I. Rossetti and E. Bahadori are grateful to Fondazione Cariplo and Regione Lombardia for financial support through the grant 2016-0858—Up-Unconventional Photoreactors.

Acknowledgments: We would like to acknowledge the Erasmus Placement program for the scholarship attributed to M. Compagnoni supporting the internship at the Cardiff Catalysis Institute (Cardiff University).

Conflicts of Interest: The authors declare no conflicts of interest.

References

1. Olivo, A.; Trevisan, V.; Ghedini, E.; Pinna, F.; Bianchi, C.L.; Naldoni, A.; Cruciani, G.; Signoretto, M. CO_2 photoreduction with water: Catalyst and process investigation. *J. CO_2 Util.* **2015**, *12*, 86–94. [CrossRef]
2. Liu, L.; Jiang, Y.; Zhao, H.; Chen, J.; Cheng, J.; Yang, K.; Li, Y. Engineering coexposed [001] and [101] facets in oxygen-deficent TiO_2 nanocrystals for enhanced CO_2 photoreduction under visble light. *ACS Catal.* **2016**, *6*, 1097–1108. [CrossRef]

3. Tahir, M.; Tahir, B.; Amin, N.A.S. Gold-nanoparticle-modified TiO_2 nanowires for plasmon enhanced photocatalytic CO_2 reduction with H_2 under visible light irradiation. *Appl. Surf. Sci.* **2015**, *356*, 1289–1299. [CrossRef]
4. Li, G.; Ciston, S.; Saponjic, Z.V.; Chen, L.; Dimitrijevic, N.M.; Rajh, T.; Gray, K.A. Synthesizing mixed-phase TiO_2 nanocomposites using a hydrothermal method for photo-oxidation and photoreduction applications. *J. Catal.* **2008**, *253*, 105–110. [CrossRef]
5. Galli, F.; Compagnoni, M.; Vitali, D.; Pirola, C.; Bianchi, C.L.; Villa, A.; Prati, L.; Rossetti, I. CO_2 photoreduction at high pressure to both gas and liquid products over titanium dioxide. *Appl. Catal. B Environ.* **2017**, *200*, 386–391. [CrossRef]
6. Corma, A.; Garcia, H. Photocatalytic reduction of CO_2 for fuel production: Possibilities and challenges. *J. Catalysis* **2013**, *308*, 168–175. [CrossRef]
7. Ohtani, B. Photocatalysis A to Z—What we know and what we do not know in a scientific sense. *J. Photochem. Photobiol. C Photochem. Rev.* **2010**, *11*, 157–178. [CrossRef]
8. Habisreutinger, S.N.; Schmidt-Mende, L.; Stolarczyk, J.K. Photocatalytic Reduction of CO_2 on TiO_2 and Other Semiconductors. *Angew. Chem. Int. Ed.* **2013**, *52*, 7372–7408. [CrossRef] [PubMed]
9. Low, J.; Qiu, S.; Xu, D.; Jiang, C.; Cheng, B. Direct evidence and enhancement of surface plasmon resonance effect on Ag-loaded TiO_2 nanotube arrays for photocatalytic CO_2 reduction. *Appl. Surf. Sci.* **2018**, *434*, 423–432. [CrossRef]
10. Mele, G.; Annese, C.; de Riccardis, A.; Fusco, C.; Palmisano, L.; Vasapollo, G.; D'Accolti, L. Turning lipophilic phthalocyanines/TiO_2 composites into efficient photocatalysts for the conversion of CO_2 into formic acid under UV–vis light irradiation. *Appl. Catal. A General* **2014**, *481*, 169–172. [CrossRef]
11. Prati, L.; Villa, A. The Art of Manufacturing Gold Catalysts. *Catalysts* **2012**, *2*, 24–37. [CrossRef]
12. Dimitratos, N.; Villa, A.; Bianchi, C.L.; Prati, L.; Makkee, M. Gold on titania: Effect of preparation method in the liquid phase oxidation. *Appl. Catal. A Gen.* **2006**, *311*, 185–192. [CrossRef]
13. Villa, A.; Ferri, D.; Campisi, S.; Chan-Thaw, C.E.; Lu, Y.; Kröcher, O.; Prati, L. Operando Attenuated Total Reflectance FTIR Spectroscopy: Studies on the Different Selectivity Observed in Benzyl Alcohol Oxidation. *ChemCatChem* **2015**, *7*, 2534–2541. [CrossRef]
14. Compagnoni, M.; Kondrat, S.A.; Chan-Thaw, C.E.E.; Morgan, D.J.; Wang, D.; Prati, L.; Dimitratos, N.; Rossetti, I. Spectroscopic Investigation of Titania-Supported Gold Nanoparticles Prepared by a Modified Deposition/Precipitation Method for the Oxidation of CO. *ChemCatChem* **2016**, *8*, 12. [CrossRef]
15. Rossetti, I.; Villa, A.; Compagnoni, M.; Prati, L.; Ramis, G.; Pirola, C.; Bianchi, C.L.; Wang, W.; Wang, D. CO_2 photoconversion to fuels under high pressure: effect of TiO_2 phase and of unconventional reaction conditions. *Catal. Sci. Technol.* **2015**, *5*, 4481–4487. [CrossRef]
16. Rossetti, I.; Villa, A.; Pirola, C.; Prati, L.; Ramis, G. A novel high-pressure photoreactor for CO_2 photoconversion to fuels. *RSC Adv.* **2014**, *4*, 28883–28885. [CrossRef]
17. Delavari, S.; Amin, N.A.S. An optimization approach for long term investments planning in energy. *Appl. Energy* **2014**, *162*, 1171–1185. [CrossRef]
18. Compagnoni, M.; Bahdori, E.; Tripodi, A.; Villa, A.; Pirola, C.; Prati, L.; Ramis, G.; Dimitratos, N.; Wang, D.; Rossetti, I. High Pressure CO_2 Photoreduction using Au/TiO_2: unravelling the effect of the co-catalyst and of the titania polymorph. *J. Mater. Chem. A*. submitted.
19. Yuzawa, H.; Yoshida, T.; Yoshida, H. Gold nanoparticles on titanium oxide effective for photocatalytic hydrogen formation under visible light. *Appl. Catal. B Environ.* **2012**, *115–116*, 294–302. [CrossRef]
20. Lari, G.M.; Nowicka, E.; Morgan, D.J.; Kondrat, S.a.; Hutchings, G. The use of carbon monoxide as a probe molecule in spectroscopic studies for determination of exposed gold sites on TiO_2. *J. Phys. Chem. Chem. Phys.* **2015**, *17*, 23236–23244. [CrossRef]
21. Liu, G.; Hoivik, N.; Wang, K.; Jakobsen, H. Engineering TiO_2 nanomaterials for CO_2 conversion/solar fuels. *Sol. Energy Mater. Sol. Cells* **2012**, *105*, 53–68. [CrossRef]
22. Raskó, J. FTIR study of the photoinduced dissociation of CO_2 on titania supported noble metals. *Catal. Letters* **1998**, *56*, 11–15. [CrossRef]
23. Rasko, J.; Solymosi, F. Infrared Spectroscopic Study of the Photoinduced Activation of CO_2 on TiO_2 and Rh/TiO_2 Catalysts. *J. Phys. Chem.* **1994**, *98*, 7147–7152. [CrossRef]

24. Indrakanti, V.P.; Kubicki, J.D.; Schobert, H.H. Photoinduced activation of CO_2 on Ti-based heterogeneous catalysts: Current state, chemical physics-based insights and outlook. *Energy Environ. Sci.* **2009**, *2*, 745. [CrossRef]
25. Ramis, G.; Busca, G.; Lorenzelli, V. Structural effects on the adsorption of alcohols on titanium dioxide. *J. Chem. Soc. Faraday Trans. 1 Phys. Chem. Condens. Phases* **1987**, *83*, 1591–1599. [CrossRef]
26. Busca, G.; Montanari, T.; Resini, C.; Ramis, G.; Costantino, U. Hydrogen from alcohols: IR and flow reactor studies. *Catal. Today* **2009**, *143*, 2–8. [CrossRef]
27. Ramis, G.; Busca, G.; Lorenzelli, V. Low temperature CO_2 adsorpion on metal oxides: spectroscopic characterization of some weakly adsoebed species. *Mater. Chem. Phys.* **1991**, *29*, 425–435. [CrossRef]
28. Busca, G.; Lorenzelli, V. Infrared spectroscopic identification of species arising from reactive adsorption of carbon oxides on metal oxide surfaces. *Mater. Chem.* **1982**, *7*, 89–126.
29. Neatu, S.; Macià-Agullò, J.A.; Concepciòn, P.; Garcia, H. Gold–Copper Nanoalloys Supported on TiO_2 as Photocatalysts for CO_2 Reduction by Water. *J. Am. Chem. Soc.* **2014**, *136*, 15969–15976. [CrossRef]
30. Liao, L.; Lien, C.; Shieh, D.; Chen, M.; Lin, J. FTIR Study of Adsorption and Photoassisted Oxygen Isotopic Exchange of Carbon Monoxide, Carbon Dioxide, Carbonate, and Formate on TiO_2. *J. Phys. Chem. B* **2002**, *106*, 11240–11245. [CrossRef]
31. Liu, L.; Zhao, H.; Andino, J.M.; Li, Y. Photocatalytic CO_2 Reduction with H2O on TiO_2 Nanocrystals: Comparison of Anatase, Rutile, and Brookite Polymorphs and Exploration of Surface Chemistry. *ACS Catal.* **2012**, *2*, 1817–1828. [CrossRef]
32. Su, W.; Zhang, J.; Feng, Z.; Chen, T.; Ying, P.; Li, C. Surface Phases of TiO_2 Nanoparticles Studied by UV Raman Spectroscopy and FT-IR Spectroscopy. *J. Phys. Chem. C* **2008**, *112*, 7710–7716. [CrossRef]
33. Collins, S.E.; Baltanás, M.a.; Bonivardi, A.L. Infrared Spectroscopic Study of the Carbon Dioxide Adsorption on the Surface of Ga2O3 Polymorphs. *J. Phys. Chem. B* **2006**, *110*, 5498–5507. [CrossRef] [PubMed]
34. László, B.; Baán, K.; Varga, E.; Oszkó, A.; Erdőhelyi, A.; Kónya, Z.; Kiss, J. Photo-induced reactions in the CO_2-methane system on titanate nanotubes modified with Au and Rh nanoparticles. *Appl. Catal. B Environ.* **2016**, *199*, 473–484. [CrossRef]
35. Chen, L.; Graham, M.E.; Li, G.; Gentner, D.R.; Dimitrijevic, N.M.; Gray, K.A. Photoreduction of CO_2 by TiO_2 nanocomposites synthesized through reactive direct current magnetron sputter deposition. *Thin Solid Films* **2009**, *517*, 5641–5645. [CrossRef]
36. Liu, L.; Gao, F.; Zhao, H.; Li, Y. Tailoring Cu valence and oxygen vacancy in Cu/TiO_2 catalysts for enhanced CO_2 photoreduction efficiency. *Appl. Catal. B Environ.* **2013**, *134–135*, 349–358. [CrossRef]
37. Compagnoni, M.; Ramis, G.; Freyria, F.S.; Armandi, M.; Bonelli, B.; Rossetti, I. Innovative photoreactors for unconventional photocatalytic processes: the photoreduction of CO_2 and the photo-oxidation of ammonia. *Rend. Lincei* **2017**, *28*, S151. [CrossRef]
38. Burcham, L.J.; Badlani, M.; Wachs, I.E. The Origin of the Ligand Effect in Metal Oxide Catalysts: Novel Fixed-Bed in Situ Infrared and Kinetic Studies during Methanol Oxidation . *J. Catal.* **2001**, *203*, 104–121. [CrossRef]
39. Whiting, G.T.; Kondrat, S.A.; Hammond, C.; Dimitratos, N.; He, Q.; Morgan, D.J.; Dummer, N.F.; Bartley, J.K.; Kiely, C.J.; Taylor, S.H.; et al. Methyl Formate Formation from Methanol Oxidation Using Supported Gold–Palladium Nanoparticles. *ACS Catal.* **2015**, *5*, 637–644. [CrossRef]
40. Montanari, T.; Sisani, M.; Nocchetti, M.; Vivani, R.; Delgado, M.C.H.; Ramis, G.; Busca, G.; Costantino, U. Zinc–aluminum hydrotalcites as precursors of basic catalysts: Preparation, characterization and study of the activation of methanol. *Catal. Today* **2010**, *152*, 104–109. [CrossRef]
41. Greaves, J.; Al-Mazroai, L.; Nuhu, A.; Davies, P.; Bowker, M. Photocatalytic methanol reforming on Au/TiO_2 for hydrogen production. *Gold Bull.* **2006**, *39*, 216–219. [CrossRef]
42. Martinez-Ramirez, Z.; Flores-Escamilla, G.A.; Berumen-España, G.S.; Jimenez-Lam, S.A.; Handy, B.E.; Cardenas-Galindo, M.G.; Sarmiento-Lopez, A.G.; Fierro-Gonzalez, J.C. Methanol carbonylation catalyzed by TiO_2–supported gold: An in-situ infrared spectroscopic investigation. *Appl. Catal. A Gen.* **2015**, *502*, 254–261. [CrossRef]
43. Calzada, L.A.; Collins, S.E.; Han, C.W.; Ortalan, V.; Zanella, R. Synergetic effect of bimetallic $Au-Ru/TiO_2$ catalysts for complete oxidation of methanol. *Appl. Catal. B Environ.* **2017**, *207*, 79–92. [CrossRef]

44. Kähler, K.; Holz, M.C.; Rohe, M.; Strunk, J.; Muhler, M. Probing the Reactivity of ZnO and Au/ZnO Nanoparticles by Methanol Adsorption: A TPD and DRIFTS Study. *ChemPhysChem* **2010**, *11*, 2521–2529. [CrossRef] [PubMed]
45. Manzoli, M.; Chiorino, A.; Boccuzzi, F. Decomposition and combined reforming of methanol to hydrogen: a FTIR and QMS study on Cu and Au catalysts supported on ZnO and TiO_2. *Appl. Catal. B Environ.* **2005**, *57*, 201–209. [CrossRef]
46. Li, M.; Li, S.; Zhang, C.; Wang, S.; Ma, X.; Gong, J. Ethanol steam reforming over Ni/NixMg1−xO: Inhibition of surface nickel species diffusion into the bulk. *Int. J. Hydrog. Energy* **2011**, *36*, 326–332. [CrossRef]
47. Maira, A.; Coronado, J.; Augugliaro, V.; Yeung, K.; Conesa, J.; Soria, J. Fourier transform infrared study of the performance of nanostructured TiO_2 particles for the photocatalytic oxidation of gaseous toluene. *J. Catalysis* **2001**, *202*, 413–420. [CrossRef]
48. Linsebigler, A.L.; Linsebigler, A.L.; Jr, J.T.Y.; Lu, G.; Lu, G.; Yates, J.T. Photocatalysis on TiO_2 Surfaces: Principles, Mechanisms, and Selected Results. *Chem. Rev.* **1995**, *95*, 735–758. [CrossRef]
49. Karakas, G.; Yetisemiyen, P. Room Temperature Photocatalytic Oxidation of Carbon Monoxide Over Pd/TiO_2–SiO2 Catalysts. *Top. Catal.* **2013**, *56*, 1883–1891. [CrossRef]
50. Orlov, A.; Jefferson, D.A.; Macleod, N.; Lambert, R.M. Photocatalytic properties of TiO_2 modified with gold nanoparticles in the degradation of 4-chlorophenol in aqueous solution. *Catal. Let.* **2004**, *92*, 41–47. [CrossRef]
51. Min, B.K.; Friend, C.M. Heterogeneous gold-based catalysis for green chemistry: low-temperature CO oxidation and propene oxidation. *Chem. Rev.* **2007**, *107*, 2709–2724. [CrossRef] [PubMed]
52. Fujishima, A.; Zhang, X.; Tryk, D. TiO_2 photocatalysis and related surface phenomena. *Surf. Sci. Rep.* **2008**, *63*, 515–582. [CrossRef]
53. Blount, M.; Falconer, J. Steady-state surface species during toluene photocatalysis. *Appl. Catal. B Environ.* **2002**, *39*, 39–50. [CrossRef]
54. Uner, D.; Oymak, M.M. On the mechanism of photocatalytic CO_2 reduction with water in the gas phase. *Catal. Today* **2012**, *181*, 82–88. [CrossRef]
55. Liu, L.; Zhao, C.; Pitts, D.; Zhao, H.; Li, Y. CO_2 photoreduction with H_2O vapor by porous MgO–TiO_2 microspheres: effects of surface MgO dispersion and CO_2 adsorption–desorption dynamics. *Catal. Sci. Technol.* **2014**, *4*, 1539. [CrossRef]
56. Wang, C.; Thompson, R.L.; Ohodnicki, P.; Baltrus, J.; Matranga, C. Size-dependent photocatalytic reduction of CO_2 with PbS quantum dot sensitized TiO_2 heterostructured photocatalysts. *J. Mater. Chem.* **2011**, *21*, 13452–13457. [CrossRef]
57. Li, K.; An, X.; Park, K.H.; Khraisheh, M.; Tang, J. A critical review of CO_2 photoconversion: catalysts and reactors. *Catal. Today* **2014**, *224*, 3–12. [CrossRef]
58. Dozzi, M.V.; Prati, L.; Canton, P.; Selli, E. Effects of gold nanoparticles deposition on the photocatalytic activity of titanium dioxide under visible light. *Phys. Chem. Chem. Phys.* **2009**, *11*, 7171–7180. [CrossRef]

© 2018 by the authors. Licensee MDPI, Basel, Switzerland. This article is an open access article distributed under the terms and conditions of the Creative Commons Attribution (CC BY) license (http://creativecommons.org/licenses/by/4.0/).